Role of Deterministic Electromechanical Conversion for Short-Term Fluctuations in Wind Power: A Case Study in Japan

Fredrik Raak,[1,*] Yoshihiko Susuki,[2,†] Shinya Eguchi,[3] and Takashi Hikihara[1]

[1]*Department of Electrical Engineering, Kyoto University, Katsura, Nishikyo-ku, Kyoto 615-8510, Japan*
[2]*Department of Electrical and Information Systems, Osaka Prefecture University, 1-1 Gakuen-cho, Naka-ku, Sakai 599-8531, Japan*
[3]*Wind Power Engineering Co. Ltd., 3-226 Minamihama, Kamisu, Ibaraki 314-0111, Japan*

Short-term wind-speed and wind-power characteristics at an offshore wind farm located in Ibaraki Prefecture (Japan) are statistically evaluated. Three models of a wind turbine's power conversion are derived from wind-turbine measurements, for which time-domain simulation and statistical analyses of their power outputs are conducted. We show that the power fluctuations are highly affected by the deterministic electromechanical conversion system and are not solely stochastically described. We also show that aggregated output fluctuations of wind turbines are not mitigated on a second scale for variations less than about 5–6 standard deviations. This implies that large output variations of wind farms are fed into the power grid, which possibly cause both frequency and voltage fluctuations.

I. INTRODUCTION

Wind power is the fastest-growing source of renewable energy [1,2] and the largest contributor of new renewable energy (not including hydro) [3]. Solar power, which is also quickly increasing its total capacity worldwide, is ranked number two [3]. Until now, wind-power variability on the time scale of 1–6 h is recognized as the biggest challenge to power-system operation under significant wind-power penetration [4]. Such variability mainly impacts the frequency control, which aims to balance the load and consumption [5]. Fluctuations on shorter time scales become a challenge to power-grid operation and control as the penetration level increases [4,6]. It has been shown that wind power is a highly intermittent source of energy, exhibiting strong *non-Gaussian* characteristics [7,8]. In Refs. [8–10], it was shown that these non-Gaussian characteristics remain in the aggregated power, even for significantly distributed generation. This is an effect of wind-speed correlations at various temporal and spatial scales, which have been demonstrated in Ref. [11] to persist over large distances. In Ref. [12], despite the neglecting of spatial correlations, it was shown that grid frequency fluctuations exhibit highly non-Gaussian characteristics affected by the intermittent nature of renewables and electricity trading. Since the dynamics of power grids depend on the loading and the stress on critical transmission lines [13],

wind-power fluctuations potentially affect the grid-wide stability [4,6,8].

This paper investigates short-term wind-speed and wind-power fluctuations with measurements from an offshore wind farm (WF) in Ibaraki Prefecture, Japan. Currently, Japan does not have a significant amount of installed wind power: with 3 GW in 2015, it covered only about 0.5% of the total electricity demand [14]. However, wind-energy resources around Japan are excellent, with a potential annual energy production of 2700 TWh [15], in which offshore wind accounts for as much as 82%. Japan seems to share this view by regarding floating turbines for offshore wind as a promising future technology [14].

This paper looks at short-term individual and aggregated output characteristics of wind turbines (WTs) for an offshore WF in Japan. The extent to which aggregated WT fluctuations are mitigated on a WF scale is demonstrated. We show that almost megawatt- (MW) scale variations are not uncommon in the WF output on the timescale of seconds, despite the maximum distance between two WTs being about 1.5 km. For example, output variations of up to 5 standard deviations are not at all mitigated. This stands in sharp contrast to the notion of fluctuations on the scale of seconds being driven by spatially uncorrelated stochastic processes [16] and stresses the importance of thoroughly assessing the potential impact of short-term fluctuations of renewable generation. Previous studies on this subject, such as [7–9,17–19], looked at the statistics of wind-power fluctuations. In particular, [19] used a dynamic power-curve model based on a stochastic

---

*fredrik.raak@gmail.com
†susuki@eis.osakafu-u.ac.jp

differential equation. The two studies [20,21] both utilized the Kraichnan-Tennekes random sweeping hypothesis to derive models of space-time correlations of WF output fluctuations. Power fluctuations are obviously a function of wind-flow-field turbulence, which has been statistically investigated for decades. For example, so-called quadrant analysis was used in Refs. [22] and [23] to relate the third-order statistical moment to turbulent energy, which motivates the use of higher-order moments to study wind-energy turbulence (see, e.g., Refs. [24,25]). In Ref. [24], it was found that for a model WT array, the maximum fluctuation is about 30% of the mean power.

In contrast to the above studies, we utilize a nonlinear dynamic model of WTs based on the electromechanical equations governing the WT dynamics (including control actions) and on data-derived aerodynamic characteristics and we use it as a comparison to measured WT outputs. We show that power fluctuations are highly affected by the electromechanical conversion, including its control system, and thus are not solely stochastically described. The present analysis provides insight into both the benefits and limitations with this type of nonlinear dynamic model, which could potentially lead to improvements in control and modeling aspects to better replicate the wind-power fluctuations or help mitigate them.

II. DESCRIPTION OF WIND FARM

The target WF comprises seven 2-MW WTs (hub height, 60 m; rotor diameter, 80 m) close to the shore in Ibaraki Prefecture, Japan and is depicted in Fig. 1, as seen from above, where WTs are indicated by blades mounted on nacelles. The distance from land to the WTs is about 20 m, i.e., they are in immediate proximity to the shore. For this configuration, small changes in the wind direction can greatly affect the WF output. All WTs have the same specification and are so-called downwind turbines [26], for which the wind passes the nacelle before the blades, in contrast to the more common so-called upwind turbines, where the situation is the opposite. Thus, for wind blowing from the sea toward land, the WTs' rotors are facing the shore.

III. WIND-TURBINE MODELING

The mechanical power extracted by a WT is in accordance with Ref. [27] and is given as follows:

$$P_w = 0.5 c_p(\lambda, \beta) \rho A_r v_w^3, \qquad (1)$$

where the so-called tip-speed ratio λ is given by $\lambda := (\omega_t r)/v_w$, where ω_t (rad/s) is the mechanical angular velocity of the turbine rotor, c_p the power coefficient, which is a function of the tip-speed ratio λ and the pitch angle $\beta \geq 0°$, $A_r = \pi r^2$ is the area swept by the rotor (r is the rotor radius), and v_w is the wind speed (in m/s). WT power curves are generally similar and c_p can be approximated by fixing five constants a_i in the following equation [27]: $c_p(\lambda) = a_1 (a_2 \Lambda - a_3) \exp(-a_4 \Lambda)$, with $\Lambda := 1/\lambda - a_5$, for $\beta = 0$ (at or below the rated power; otherwise, β is increased to limit the power extraction). An optimal relation between P_w and ω_t, $P_w^*(\omega_t)$ is derived by tracking the maximum value of Eq. (1) for different wind and/or rotor speeds and is called maximum power point tracking (MPPT) [28]. $P_w^*(\omega_t)$ is used to control the turbine at optimal power. The power curve $P_w(v_w)$ is derived by solving

$$P_w[\lambda(v_w, \omega_t)] - P_w^*(\omega_t) = 0, \qquad (2)$$

for a number of wind speeds and is shown in Fig. 2, based on our measurements (see "Mod. Curve"). Another power curve, "Avg. Curve," which is constructed from the average of measurement data, will also be used in an evaluation of the output-power characteristics. Additionally, we use a more detailed dynamic WT model that incorporates the derived power coefficient $c_p(\lambda)$, based on a set of differential algebraic equations (DAEs) in Ref. [29] for doubly fed induction-generator (DFIG) WTs and a two-mass mechanical model [30] (see the Appendix).

IV. WIND-SPEED AND POWER STATISTICS

In this paper, we utilize 1-Hz sampled wind speeds and WT outputs measured at the WF. The wind speeds are
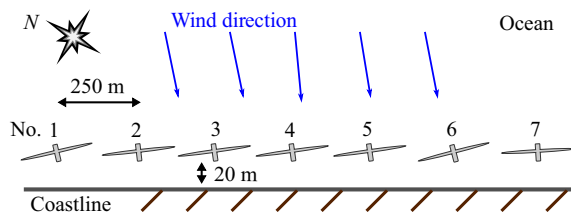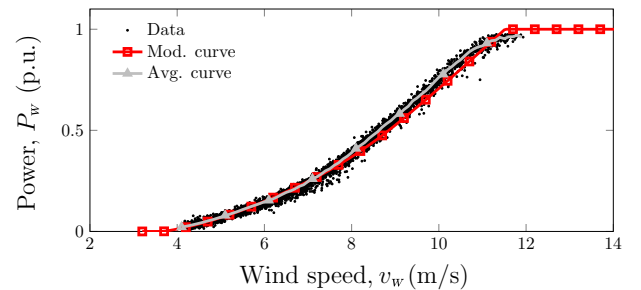
FIG. 1. A depiction of the configuration of the target WF, as seen from above. Seven WTs are placed 20 m off the coast of Ibaraki Prefecture, Japan. The distance between all WTs is 250 m. "N" in the upper left corner indicates north.

FIG. 2. Measured data and averaged and modeled power curves: "Avg. Curve" and "Mod. Curve." The modeled curve is derived using Eq. (2).

measured with cup anemometers mounted at the top of the WT nacelles (the housing of the electronic-mechanical equipment such as the generator). To statistically evaluate short-term wind-speed and power fluctuations, we decompose the wind speeds or output powers $u(t)$ as follows [9,19,31]:

$$u(t) = \langle u \rangle_T + u'(t), \tag{3}$$

where $\langle u \rangle_T$ denotes the sample mean ($\langle \cdot \rangle$ denotes the mean operation) over some period T and $u'(t)$ denotes the fluctuations (or deviations from the mean). According to the IEC standard [16], wind-speed fluctuations are defined as deviations from the $T = 10$ min averages and we use the same definition for the output power for the sake of consistency. The turbulence intensity [26] of wind is defined as $T_I := \sigma / \langle u \rangle_T$ ($T = 10$ min), where $\sigma = \sqrt{\langle u'^2 \rangle}$ is the sample standard deviation. We estimate probability density functions (PDFs) of normalized fluctuations $p(u'/\sigma)$, where p denotes the PDF, to qualitatively compare statistics of wind speed and those of measured and modeled power outputs. The associated cumulative density function (CDF) is given by $F(x) = \int_{-\infty}^{x} p(x)dx$. Furthermore, we look at increments of $u(t)$ [9], which are simply defined as follows:

$$du(t, \tau) = u(t + \tau) - u(t) = u'(t + \tau) - u'(t), \tag{4}$$

where τ is a time shift in seconds. The right-hand-side equality is true within each averaging period T. Wind-speed increments are closely related to wind gustiness [32], which affects the load on WT structures [33]. Wind-power increments are associated with *wind-power ramps*, which are often analyzed on hourly time scales and are important to predict to ensure safe power-system operation [34]. As measures for comparison and *normality* of u' and du, we look at the sample skew $Sk := \langle u'^3 \rangle / \sigma^3$ and kurtosis $Kt := \langle u'^4 \rangle / \sigma^4$. Note that for normally distributed data, we have $Sk = 0$ and $Kt = 3$. Sk quantifies asymmetry in the distribution. Kt quantifies the "thickness" of the tails of the PDF [35]; i.e., a higher value indicates a higher probability of extreme values. Now assuming $\langle u'(t)^2 \rangle = \langle u'(t + \tau)^2 \rangle$, which holds to high precision for long time series, the second moment (variance) of increments, or the so-called second-order structure function [31,36], can be written as follows:

$$\langle du(t, \tau)^2 \rangle = \langle 2u'(t)^2 - 2u'(t + \tau)u'(t) \rangle \tag{5}$$

or, equivalently, as

$$\langle du(t, \tau)^2 \rangle = 2\sigma^2 \left(1 - r_{u,u}(\tau) \right), \tag{6}$$

where we have utilized the fact that $\sigma^2 = \langle u'(t)^2 \rangle$ and that the sample autocorrelation $r_{u,u}(\tau) := \langle u'(t + \tau)u'(t) \rangle / \sigma^2$.

Hence, we see that the second moment of increments depends on the autocorrelation. Similarly, higher-order moments $\langle du^n \rangle$ depend on higher-order correlations $r_{u^{m_1}, u^{m_2}}(\tau)$ (with m_i designating the order; i.e., not the lag) [31]. These higher-order correlations are evidently manifested in the PDF since they affect the shape.

V. RESULTS AND DISCUSSIONS

Examples of 1-Hz sampled wind speeds $\tilde{v}_w$ and P'_w are shown in Fig. 3. The output power looks more "smooth" than $\tilde{v}_w$, which is due to filtering in the electromechanical conversion process and because the WT blades act as a low-pass filter for the wind. In Fig. 4(a), about 2-min-long trajectories of measured and simulated (using the dynamic model of a DFIG) P_w are plotted against v_w. It is observed that $P_w(v_w)$ approximates the long-term averaged output P_w quite well. However, it cannot capture short-term dynamics, since both the measurements and data from the dynamic simulation "Dyn. Sim." exhibit large deviations from the power curve. This is due to the controls and inertia of the WT [9,19], which are included in the utilized dynamic model. For example, examining the time series in Fig. 4(b), we see that the measured WT output and the output from the dynamic simulation fluctuate in a similar manner, which is qualitatively different from the outputs estimated with the power curves "Mod. Curve" and "Avg. Curve." Therefore, we understand that the dynamic model is necessary for the evaluation of short-term power fluctuations. This behavior has also been described as a stochastic model (Langevin process) of a power curve [9,19,37] consisting of a deterministic drift toward the
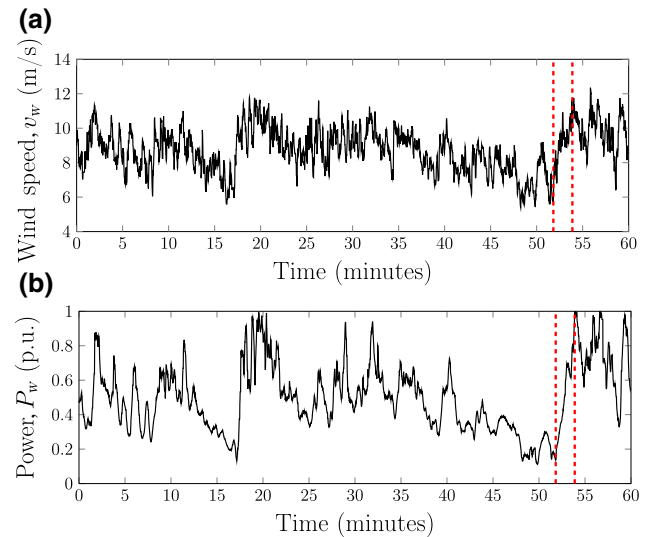

(a)

(b)

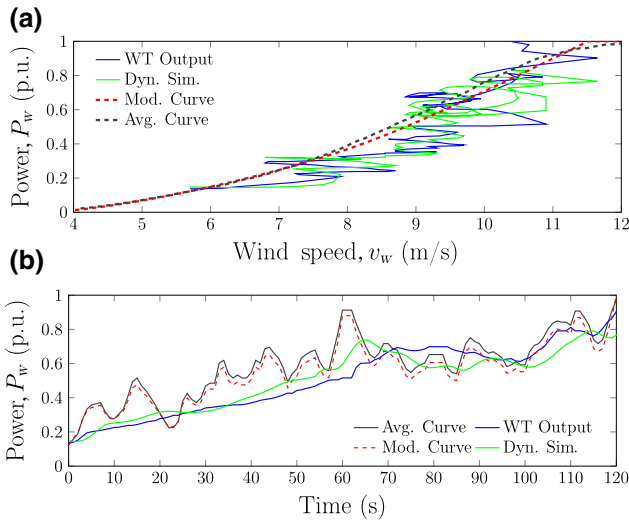FIG. 3.   A 1-h example time series of measured (a) wind speeds and (b) output powers. The interval marked in red is used in Fig. 4.

FIG. 4. Measured and simulated power outputs plotted against (a) wind speed and (b) time, for the interval indicated in red in Fig. 3.

FIG. 5. PDFs of (a) normalized fluctuations u'/σ and (b) increments $du(t, \tau)/\sigma$ ($\tau = 4$ s). The Gaussian PDFs have standard deviation $\sigma = 1$ (the same as the standard deviations of u'/σ and $du(t, \tau)/\sigma$). In (b), the PDFs are arbitrarily shifted in the y direction for the sake of easy comparison.

power curve plus Gaussian noise. For another wind-energy application and theory, see, e.g., Refs. [38,39].

To quantitatively compare the measurements and simulations, we will now look at the statistical properties of the wind-speed and wind-power fluctuations: v_w' and p_w'. The data consist of 1-Hz WT measurements acquired over a 3.6-day period. For the same period, we also look at the aggregated and normalized WF output of the WTs (see Fig. 1). Normalized PDFs of v_w', "Wind Speed," and p_w', "WT Output," are shown in Fig. 5(a). Bear in mind that fluctuations are defined as deviations from the 10-min average. It is noted that the wind speed, the WT output, the simulated outputs, and the WF output, "WF Output," all become close to the Gaussian PDF for fluctuations smaller than about 4 standard deviations (4σ) in magnitude. The simulated outputs consist of outputs from dynamic simulation of the DAE model: "Dyn. Sim." and the two power curves shown in Fig. 2.

Now, we consider PDFs of increments $du(t, \tau)$, given in Fig. 5(b) in arbitrary units (a.u.) for $\tau = 4$ s. The PDFs are shifted in the y direction for the sake of easy visual comparison. Compared to Fig. 5(a), all PDFs exhibit heavy tails, indicating non-Gaussian characteristics. In particular, we see that the PDF of WT output increments exhibits the heaviest tails, followed by dynamic simulation and total WF output. The dynamic simulation works best for replicating the heavy tail in the measured data: see also Fig. 7 and the associated discussion. The non-Gaussian PDF characteristics are influenced by nonzero higher-order autocorrelations. Evidently, these characteristics are most prevalent in the power outputs due to the nonlinear electromechanical conversion of wind to electric power. Fluctuations in the wind speed of a few meters per second
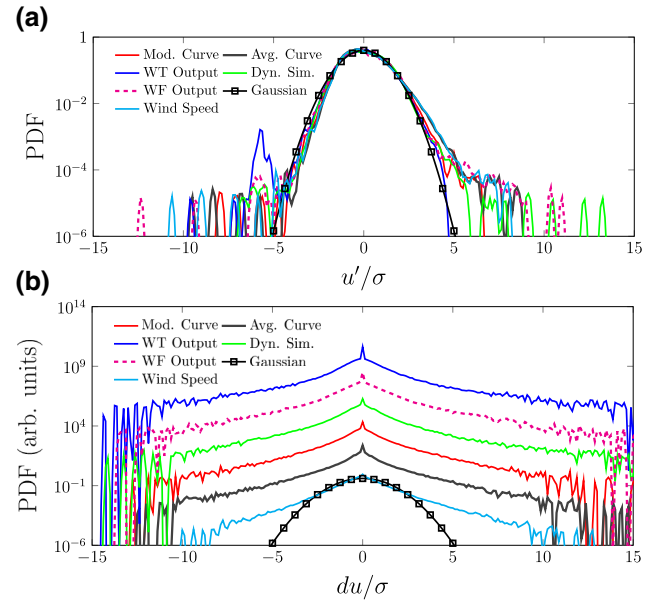
can cause large variations in the WT output, amplifying the intermittency of the wind (see, e.g., Fig. 3). We can also understand that low-pass filtering effects in the power conversion due to WT inertia and the blades increase the autocorrelation, consequently affecting the increment PDFs.

In the following, we compare output characteristics by how the second-order structure function $\langle du(t, \tau)^2 \rangle$ and the normalized third and fourth statistical moments, Sk and Kt, scale with the time shift τ. The results are shown in Fig. 6. In Fig. 6(a), we can see that "Dyn. Sim." is significantly closer to the actual wind-power output than "Mod. Curve" and that the WF output exhibits considerably different scaling characteristics for $\tau \in [10^2, 10^5]$. Note that the $\langle du(t, \tau)^2 \rangle \sim \tau^{2/3}$ scaling is the equivalent of the famous $S(f) \sim f^{-5/3}$ scaling law for the turbulence spectrum [40], which is discussed later on. Figure 6(b) demonstrates that positive values of skewness are obtained for all data and that WT output and "Dyn. Sim." give the largest values for small time shifts—orders of 1–10. The results on increment kurtosis shown in Fig. 6(c) show that "Dyn. Sim." is similar to "WT Output" and "WF Output" for $\tau \approx 2$ s and that it converges to "Mod. Curve" for $\tau > 10$ s. This is expected since the modeled power curve and the dynamical model are based on the same data-derived power coefficient c_p and the dynamic power conversion mainly affects the output characteristics on time scales of up to tens of seconds [9,40].
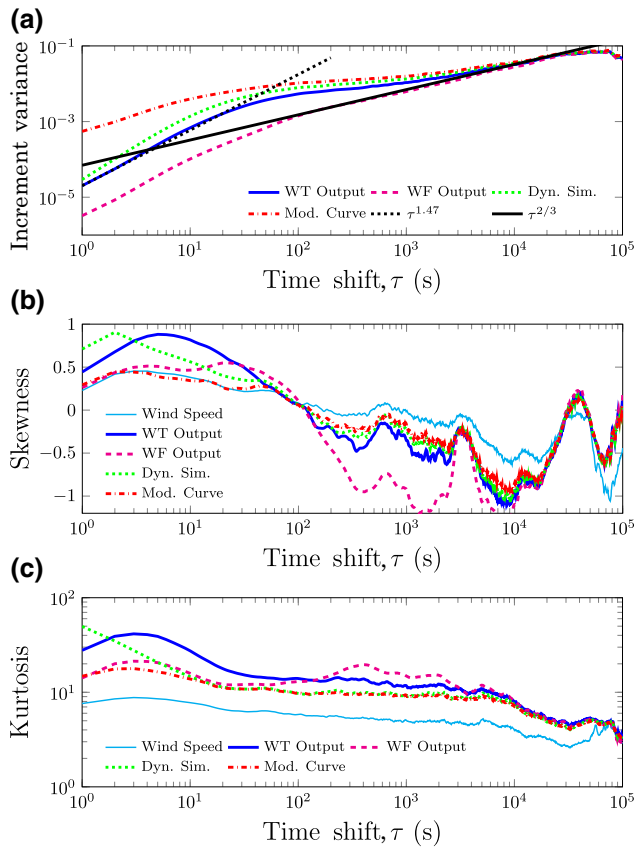
FIG. 6. (a) The second-order structure function according to Eq. (5) and the normalized third and fourth statistical moments, Sk in (a) and Kt in (b), plotted against the time shift τ.

In Fig. 7(a), cross-correlations are shown between WT outputs and "Dyn. Sim.," and "Mod. Curve" outputs (or "MC") for low-pass-filtered wind speeds as input [with different time constants T (s)]. The results show that "Dyn. Sim." and "Mod. Curve, $T = 8$ s" are close and that setting $T = 12$ s gives the highest correlation. However, Fig. 7(b), which shows Kt vs Sk of $du(t, \tau)$ with $\tau = 1$ s, ..., 100 s, demonstrates that despite the higher linear correlation, "Dyn. Sim." replicates the non-Gaussian characteristics of the measured WT output much better than the "MC" output, although it uses the same power-factor function c_p. The relation between higher-order velocity fluctuations and turbulent energy is discussed in Refs. [22–24]. In light of this, our results demonstrate that the dynamics of the conversion system modify the wind turbulence beyond simple scaling and/or filtering and consequently suggest that changes to turbine design and controls have the potential to alter turbulence characteristics. Additionally, even though "Dyn. Sim." and "WT Output" look very similar, it should be noted that they are slightly different with regard to τ: e.g., $\tau = 2$ s for "Dyn. Sim." gives a result that is roughly equivalent to $\tau = 6$ s for "WT Output" (encircled by the purple ellipse). The difference in time constant is
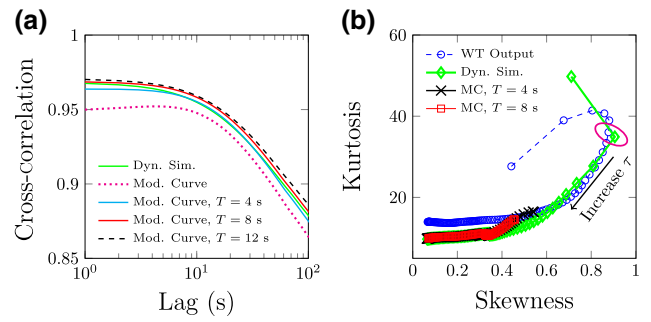

FIG. 7. (a) Cross-correlations between WT outputs and "Dyn. Sim.," and "Mod. Curve" outputs (or "MC") for low-pass-filtered wind speeds as input [with different time constants T (s)]. (b) The kurtosis vs skewness of $du(t, \tau)$ with $\tau = 1$ s, ..., 100 s. The purple ellipse encircles two points at which the trajectories of "Dyn. Sim." and "WT Output" look as though they are converging for appropriately chosen lags τ (s).

certainly related in part to the model parameters, which have not been tuned but instead set to standard values from the literature (see the Appendix).

Now, WT and WF increments are compared by looking at the probability of a certain increment x given by $P(du/\sigma > x) = 1 - F(x)$, where $F(x)$ denotes the CDF of the increments. Figure 8 shows $P(du/\sigma > x)$ for the measured and simulated WT outputs and for WF outputs for $\tau = 1$ and 8 s. These results clearly show that the probability of sudden changes in the WF and WT outputs on the time scale of seconds are very close until about 5–6 standard deviations. As an example, here, an increment of 7 standard deviations corresponds to a change in WF output of about 0.5 MW, which is quite significant; i.e., there is very little smoothing: for closed-form spatiotemporal models of turbulence coherence for WTs, see Refs. [20] and [21]. Since higher correlations are found for low-frequency
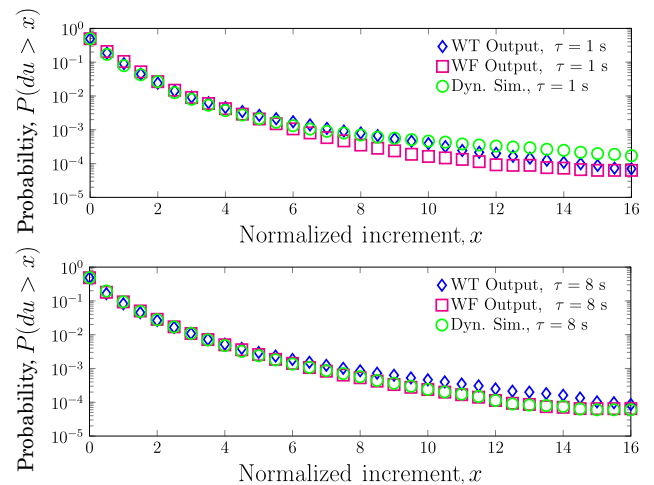

FIG. 8. The probabilities $P(du > x)$ of WT- and WF-normalized output increments $du(t, \tau)/\sigma$ larger than x.
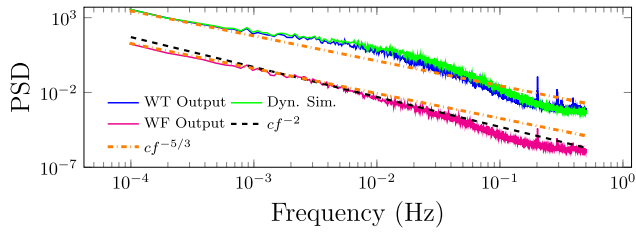
FIG. 9. The PSDs of the WF and measured and/or simulated WT outputs.

fluctuations (larger-scale atmospheric motions), the WTs here are not far enough removed from each other to induce large smoothing effects. Large WF variability as observed here is potentially challenging for power-system operation. Interestingly, the results for "Dyn. Sim." appear to be in between "WT Output" and "WF Output" for $\tau = 1$ s but for $\tau = 8$ s we see an extremely close resemblance between the output increment probabilities for "Dyn. Sim." and "WF Output." This result suggests that a part of what is not captured by the dynamic simulation may be caused by either wind fluctuations on the time scale of seconds not captured by the scalar input to the model or by the WT model itself. Further, these wind fluctuations are mitigated in the aggregated power and consequently lead to good agreement with the dynamic simulation.

Finally, we look at the power spectral density (PSD) of wind power, which has been shown to follow the so-called Kolmogorov spectrum [41] according to $S(f) \sim f^{-5/3}$; the wind-speed spectrum is similar [9]. Models of WT and WF spectra as functions of the wind turbulence have been proposed in Ref. [42]. Here, we estimate PSDs with the function PWELCH in MATLAB. PSDs of WF and measured and simulated WT outputs are shown in Fig. 9. The PSDs of the WT outputs are scaled for the sake of easy comparison. The results show two things. First, the PSDs scale fairly accurately according to Kolmogorov's spectrum; however, significant deviations from the scaling theory are observed for both moderate and high frequencies for measured and simulated WT outputs (which are close). Second, the WF spectrum scales slightly differently than the spectrum of a single WT, namely in that the WF spectra are more accurately described by the scaling $S(f) \sim f^{-2}$ over a large range of frequencies. This was also noted in Ref. [43].

VI. CONCLUSIONS

Short-term wind-speed and wind-power characteristics at an offshore wind farm located in Ibaraki Prefecture, Japan are statistically evaluated. Three models of a WT's power conversion are derived from measurements and time-domain simulation and statistical analyses are conducted. Our main conclusions and contributions are as follows. First, the results indicate that the power fluctuations

are better represented by the differential algebraic model than by standard power curves. That is, power fluctuations appear to be highly affected by the deterministic electromechanical conversion and/or control system and are not solely stochastically described. Therefore, we suggest that the development of a representative dynamic model of the WT is essential for understanding and controlling fluctuations in the short-term. Second, we show that aggregated WT output fluctuations are not mitigated on a second scale for variations less than about 5–6 standard deviations. Since the balance of active power is closely linked to the grid frequency, this implies that large WF-output variations are fed into the power system, which could possibly cause both frequency and voltage fluctuations.

APPENDIX: NONLINEAR DYNAMIC MODEL OF WIND TURBINES

The dynamics of the mechanical system are described by a two-mass model, with the two masses being the WT's rotor and generator, and are given in Ref. [30] as follows:

$$\frac{d\omega_t}{dt} = \frac{1}{2H_t}(T_t - T_g),$$
$$\frac{d\omega_g}{dt} = \frac{1}{2H_g}(T_g - T_e), \qquad (A1)$$
$$\frac{d\gamma}{dt} = \omega_b(\omega_t - \omega_g),$$

where $T_t = P_w/\omega_t$ is the turbine torque, $T_g = k_s\gamma + Dd\gamma/dt$ is the generator's mechanical torque, H_t and H_g are the turbine and generator inertia constants, k_s is the shaft stiffness, D is the damping constant, γ is the shaft twist angle, $\omega_b = 2\pi50$ rad/s, and T_e is the electrical torque. Here, typical values from Ref. [30] have been used. The set of DAEs

$$\frac{d\mathbf{x}}{dt} = \mathbf{f}_1(\mathbf{x}, \mathbf{y}, v_w),$$
$$\mathbf{0} = \mathbf{f}_2(\mathbf{x}, \mathbf{y}), \qquad (A2)$$

where v_w is the input wind speed (measurement data), is solved using a trapezoidal solver [29] employed in MATLAB, where $\mathbf{f}_1$ and $\mathbf{f}_2$ are the sets of differential and algebraic equations, respectively. The state variables are $\mathbf{x} = [v_{wf}, \omega_t, \omega_g, \gamma, \beta, i_{dr}, i_{qr}]^\top$, where i_{dr} and i_{qr} are

rotor currents in the *dq* reference frame, and v_{wf} is the low-pass-filtered wind speed (according to Ref. [27]). The equations for the mechanical input (P_w) to the model are given in Sec. III. The controllers are modeled exactly as in Refs. [29] and [44]. Except for known WT parameters such as dimensions, typical DFIG parameters are taken from Ref. [29].

———

[1] T. Ackermann, in *Wind Power in Power Systems*, edited by T. Ackermann (John Wiley & Sons, Ltd, Chichester, UK, 2012), p. 21.

[2] A. M. Foley, P. G. Leahy, A. Marvuglia, and E. J. McKeogh, Current methods and advances in forecasting of wind power generation, Renewable Energy **37**, 1 (2012).

[3] Renewable Energy Policy Network for the 21st Century (REN21): Renewables 2016 Global Status Report (Paris: REN21 Secretariat) (2016), [Online]. Available at http://www.ren21.net/wp-content/uploads/2016/06/GSR_2016_Full_Report.pdf (Last accessed on 5 June 2018).

[4] H. Holttinen, P. Meibom, A. Orths, B. Lange, M. O'Malley, J. O. Tande, A. Estanqueiro, E. Gomez, L. Söder, G. Strbac, J. C. Smith, and F. van Hulle, Impacts of large amounts of wind power on design and operation of power systems, results of IEA collaboration, Wind Energy **14**, 179 (2011).

[5] Y.-H. Wan, M. Milligan, and B. Parsons, Output power correlation between adjacent wind power plants, J. Sol. Energy Eng. **125**, 551 (2003).

[6] D. Flynn, Z. Rather, A. Ardal, S. D'Arco, A. Hansen, N. Cutululis, P. Sorensen, A. Estanquiero, E. Gómez, N. Menemenlis, C. Smith, and Y. Wang, Technical impacts of high penetration levels of wind power on power system stability, Wiley Interdiscip. Rev.: Energy Environ. **6**, e216 (2017).

[7] J. Gottschall and J. Peinke, Stochastic modelling of a wind turbine's power output with special respect to turbulent dynamics, J. Phys.: Conf. Ser. **75**, 012045 (2007).

[8] M. Anvari, G. Lohmann, M. Wächter, P. Milan, E. Lorenz, D. Heinemann, M. R. R. Tabar, and J. Peinke, Short term fluctuations of wind and solar power systems, New J. Phys. **18**, 063027 (2016).

[9] P. Milan, M. Wächter, and J. Peinke, Turbulent Character of Wind Energy, Phys. Rev. Lett. **110**, 138701 (2013).

[10] O. Kamps, in *Wind Energy—Impact of Turbulence*, edited by M. Hölling, J. Peinke, and S. Ivanell (Springer, Berlin, Heidelberg, 2014), p. 67.

[11] R. Baïle and J.-F. Muzy, Spatial Intermittency of Surface Layer Wind Fluctuations at Mesoscale Range, Phys. Rev. Lett. **105**, 254501 (2010).

[12] B. Schäfer, C. Beck, K. Aihara, D. Witthaut, and M. Timme, Non-Gaussian power grid frequency fluctuations characterized by Lévy-stable laws and superstatistics, Nat. Energy **3**, 119 (2018).

[13] N. W. Miller, Keeping it together: Transient stability in a world of wind and solar generation, IEEE Power Energy Mag. **13**, 31 (2015).

[14] Global Wind Energy Council (GWEC): Global Wind Report Annual Market Update (2016), [Online]. Available at http://www.gwec.net/global-figures/graphs/ (Last accessed on 5 June 2018).

[15] X. Lu, M. B. McElroy, and J. Kiviluoma, Global potential for wind-generated electricity, Proc. Natl. Acad. Sci. **106**, 10933 (2009).

[16] International Electrotechnical Commission (IEC): IEC 61400-1 Wind turbine generator systems—Part 1: Design requirements (2005).

[17] R. Calif, F. G. Schmitt, and Y. Huang, Multifractal description of wind power fluctuations using arbitrary order Hilbert spectral analysis, Physica A: Stat. Mech. Appl. **392**, 4106 (2013).

[18] R. Calif and F. G. Schmitt, Multiscaling and joint multiscaling of the atmospheric wind speed and the aggregate power output from a wind farm, Nonlinear Process. Geophys. **21**, 379 (2014).

[19] P. Milan, M. Wächter, and J. Peinke, Stochastic modeling and performance monitoring of wind farm power production, J. Renewable Sustainable Energy **6**, 033119 (2014).

[20] N. Tobin and L. P. Chamorro, Turbulence coherence and its impact on wind-farm power fluctuations, J. Fluid Mech. **855**, 1116 (2018).

[21] L. J. Lukassen, R. J. Stevens, C. Meneveau, and M. Wilczek, Modeling space-time correlations of velocity fluctuations in wind farms, Wind Energy **21**, 474 (2018).

[22] H. Nakagawa and I. Nezu, Prediction of the contributions to the Reynolds stress from bursting events in open-channel flows, J. Fluid Mech. **80**, 99 (1977).

[23] M. Raupach, Conditional statistics of Reynolds stress in rough-wall and smooth-wall turbulent boundary layers, J. Fluid Mech. **108**, 363 (1981).

[24] K. Viestenz and R. B. Cal, Streamwise evolution of statistical events in a model wind-turbine array, Boundary Layer Meteorol. **158**, 209 (2016).

[25] N. Ali, A. S. Aseyev, and R. B. Cal, Structure functions, scaling exponents and intermittency in the wake of a wind turbine array, J. Renewable Sustainable Energy **8**, 013304 (2016).

[26] J. Manwell, J. McGowan, and A. Rogers, *Wind Energy Explained: Theory, Design and Application* (John Wiley & Sons, Chichester, UK, 2009).

[27] K. Elkington, J. G. H. Slootweg, M. Ghandhari, and W. L. Kling, in *Wind Power in Power Systems*, edited by T. Ackermann (John Wiley & Sons, Ltd, Chichester, UK, 2012), p. 821.

[28] E. Koutroulis and K. Kalaitzakis, Design of a maximum power tracking system for wind-energy-conversion applications, IEEE Trans. Ind. Electron. **53**, 486 (2006).

[29] F. Milano, *Power System Modelling and Scripting* (Springer, London, UK, 2010).

[30] F. Mei and B. Pal, Modal analysis of grid-connected doubly fed induction generators, IEEE Trans. Energy Convers. **22**, 728 (2007).

[31] A. Morales, M. Wächter, and J. Peinke, Characterization of wind turbulence by higher-order statistics, Wind Energy **15**, 391 (2012).

[32] F. Böttcher, C. Renner, H.-P. Waldl, and J. Peinke, On the statistics of wind gusts, Boundary Layer Meteorol. **108**, 163 (2003).

[33] F. K. Davis and H. Newstein, The variation of gust factors with mean wind speed and with height, J. Appl. Meteorol. **7**, 372 (1968).

[34] A. Bossavy, R. Girard, and G. Kariniotakis, Forecasting ramps of wind power production with numerical weather prediction ensembles, Wind Energy **16**, 51 (2013).

[35] L. T. DeCarlo, On the meaning and use of kurtosis, Psychol. Methods **2**, 292 (1997).

[36] F. Anselmet, Y. Gagne, E. Hopfinger, and R. Antonia, High-order velocity structure functions in turbulent shear flows, J. Fluid Mech. **140**, 63 (1984).

[37] T. A. Mücke, M. Wächter, P. Milan, and J. Peinke, Langevin power curve analysis for numerical wind energy converter models with new insights on high frequency power performance, Wind Energy **18**, 1953 (2015).

[38] M. S. Melius, M. Tutkun, and R. B. Cal, Solution of the Fokker-Planck equation in a wind turbine array boundary layer, Physica D: Nonlinear Phenom. **280**, 14 (2014).

[39] M. Ragwitz and H. Kantz, Indispensable Finite Time Corrections for Fokker-Planck Equations from Time Series Data, Phys. Rev. Lett. **87**, 254501 (2001).

[40] M. M. Bandi, Spectrum of Wind Power Fluctuations, Phys. Rev. Lett. **118**, 028301 (2017).

[41] J. Apt, The spectrum of power from wind turbines, J. Power Sources **169**, 369 (2007).

[42] H. Liu, Y. Jin, N. Tobin, and L. P. Chamorro, Towards uncovering the structure of power fluctuations of wind farms, Phys. Rev. E **96**, 063117 (2017).

[43] J. Bossuyt, C. Meneveau, and J. Meyers, Wind farm power fluctuations and spatial sampling of turbulent boundary layers, J. Fluid Mech. **823**, 329 (2017).

[44] F. Milano, An open source power system analysis toolbox, IEEE Trans. Power Syst. **20**, 1199 (2005).